metals

MDPI

Article

Analyzing the Precipitation Effects in Low-Alloyed Copper Alloys Containing Hafnium and Chromium

Julia Dölling [1,*], Moritz Kuglstatter [2], Ulrich Prahl [3], Heinz Werner Höppel [2], Patrick Ortner [2], Benedict Ott [2], Stefanie Felicia Kracun [4], Martin Fehlbier [4] and Andreas Zilly [1]

[1] Faculty of Technology, Cooperative State University Stuttgart, Lerchenstr. 1, 70174 Stuttgart, Germany
[2] Department of Materials Science & Engineering, Institute I: General Materials Properties, Friedrich-Alexander-Universität Erlangen-Nürnberg, Martensstr. 5, 91058 Erlangen, Germany; moritz.kuglstatter@fau.de (M.K.); patrick.p.ortner@fau.de (P.O.); benedict.ott@fau.de (B.O.)
[3] Institute of Metal Forming, TU Bergakademie Freiberg, Bernhard-von-Cotta-Str. 4, 09599 Freiberg, Germany
[4] Department for Casting-Technology (GTK), University Kassel, Kurt-Wolters-Str. 3, 34125 Kassel, Germany; s.kracun@uni-kassel.de (S.F.K.)
* Correspondence: julia.doelling@dhbw-stuttgart.de

Abstract: Copper alloys containing chromium and hafnium combine elevated mechanical strength and high electrical and thermal conductivity. For the simultaneous enhancement of both material properties, precipitation hardening is the utilized mechanism. Therefore, the aim is to analyze the influence of chromium and hafnium in binary and ternary low-alloyed copper alloys and to compare the precipitation processes during temperature exposure. Atom probe tomography (APT) and differential scanning calorimetry (DSC) measurements enable to understand the precipitation sequence in detail. CuCr0.7 starts to precipitate directly, whereas CuHf0.7 is highly influenced by prior diffusion facilitating cold rolling. Within the ternary alloy, hafnium atoms accumulate at the shell of mainly Cr-containing precipitates. Increasing the local hafnium concentration results in the formation of intermetallic CuHf precipitates at the sites of mainly Cr-containing precipitates. Indirect methods are utilized to investigate the materials' properties and show the impact of cold rolling prior to an aging treatment on binary alloys CuCr and CuHf. Finally, ternary alloys combine the benefits of facilitated precipitation processes and decelerated growing and coarsening, which classifies the alloys to be applicable for usage at elevated temperatures.

Keywords: copper–hafnium CuHf; copper–chromium CuCr; CuHfCr; atom probe tomography APT; differential scanning calorimetry DSC; precipitation hardening; precipitation mechanism; cold working; cold rolling; conductivity improvement; high-performance copper alloy; conduction materials; electrical and automotive engineering

check for updates

Citation: Dölling, J.; Kuglstatter, M.; Prahl, U.; Höppel, H.W.; Ortner, P.; Ott, B.; Kracun, S.F.; Fehlbier, M.; Zilly, A. Analyzing the Precipitation Effects in Low-Alloyed Copper Alloys Containing Hafnium and Chromium. *Metals* **2024**, *14*, 258. https://doi.org/10.3390/met14030258

Academic Editor: Antoni Roca

Received: 12 January 2024
Revised: 9 February 2024
Accepted: 15 February 2024
Published: 22 February 2024

Copyright: © 2024 by the authors. Licensee MDPI, Basel, Switzerland. This article is an open access article distributed under the terms and conditions of the Creative Commons Attribution (CC BY) license (https://creativecommons.org/licenses/by/4.0/).

1. Introduction

Copper alloys for high-performance applications require a favorable combination of high electrical and thermal conductivity as well as enhanced mechanical properties. Precipitation hardening enables increase in these properties during an aging treatment simultaneously. For high electrical conductivity, the solute amount of alloying elements is the most crucial factor due to conduction electron scattering [1–3]. Therefore, target-oriented usage of precipitation hardening is an important hardening mechanism for current and future applications of copper alloys in the automotive and electronic industries.

In general, precipitation hardening alloys need to have a limited and with temperature decreasing solubility in the copper matrix [4]. This is why CuCr1Zr is a commonly used low-alloyed copper alloy for challenging applications [5]. Additions of hafnium appear to provide beneficial mechanical properties [2,6,7]. Nevertheless, the precipitation sequence has not been analyzed in-depth for ternary copper alloying concepts.

1.1. Precipitation of Binary Alloys: CuCr

Chromium enables beneficial precipitation reactions with a maximum solubility of 0.65 wt.% in copper at 1075 °C, decreasing with temperature [8,9].

A similar atomic radius of chromium and copper supports the diffusion and the nucleation of spherical mainly Cr-containing precipitates, which grow rapidly and are homogenously distributed without preferred sites [10,11]. During the reaction, the activation energy for a growth-capable fcc nucleus is beneficial [12], whereas the continuously growing precipitates later strive for their stable bcc equilibrium structure [10,11,13,14]. For larger incoherent precipitates (8–10 nm), the Orowan mechanism contributes to the strengthening effect, whereas the cutting mechanism dominates for smaller particles (3–4.5 nm) [15–17].

For CuCr0.7, it is possible to follow precipitation reactions during DSC measurements [6,18,19], including several exothermic peaks related to solid-state reactions. Optional cold rolling prior to the aging process is beneficial for accelerated reactions, but generally, the most significant impact during heat treatments is the aging temperature [6].

Resulting properties span the possible hardness in the range of 150 HV to 180 HV and electrical conductivity of 40 MS/m to about 54 MS/m, which underlines the usage of CuCr systems in a wide field of applications [2,5,20,21]. The usage of further alloying elements will provide elevated properties and advanced performance.

1.2. Ternary Alloys: CuCrZr

CuCrZr is an industrially commonly used alloy due to its favorable combination of mechanical properties, electrical conductivity, and relaxation behavior at elevated temperatures. Alloying with zirconium mainly affects the growth of Cr-containing precipitates [22–24] because the Zr atoms tend to diffuse into the interface between the Cr-containing precipitate and the Cu matrix [22,24]. Because of the accumulation of foreign atoms at this interface, the elastic stresses are reduced due to the geometric misfit, which improves the mechanical properties and helps the thermal stability against Ostwald ripening with decreasing mechanical properties [25]. A comparable behavior is reported for magnesium, iron, and silicon [24].

1.3. Precipitation of Binary Alloys: CuHf

Hafnium has, with 0.84 wt.% at 963 °C, a limited and, with temperature, rapidly decreasing solubility in copper [26,27]. Due to a similar thermomechanical behavior, CuHf alloys are often compared with CuZr and CuTi alloys [28–30].

The latest research on the precipitation mechanism in a binary CuHf0.9 alloy shows how Guinier Preston (GP) zones form during aging treatments (for example, 1 h at 450 °C) and result in spherical Cu_5Hf phases which are coherent to the surrounding copper matrix ($(111)_{Cu}//(311)_{Cu5Hf}$ with $[0\bar{1}1]_{Cu}//[0\bar{1}1]_{Cu5Hf}$) [25]. Continuing aging treatment results in growing precipitates which change their crystallographic structure in an exothermic solid state reaction [6] from cubic Cu_5Hf to hexagonal closed-packed $Cu_{51}Hf_{14}$ phase at a critical radius of 9.5 nm [25]. This second phase grows in rod-shaped morphology, losing its coherency to the copper matrix [25].

Higher aging temperatures and facilitated diffusion are beneficial for the precipitation processes [2,6], and cold rolling accelerates precipitation reactions at lower temperatures [6]. In many cases, cold deformation of supersaturated metals is applied before aging heat treatments. This results in homogenously distributed precipitates of smaller size [31]. Numerous crystallographic defects provide heterogeneous nucleation sites, lower the necessary activation energy [32–35], and facilitate diffusive atom movement along dislocations [32,36].

Overall, CuHf alloys appear to provide interesting properties such as 130 HV 0.1 to 190 HV 0.1 at 35 MS/m to 45 MS/m [7,27,37].

1.4. Ternary Alloys: CuCrHf

Alloying CuCr with small amounts of hafnium has generally resulted in promising mechanical performance and good electrical conductivity, especially in combination with thermal and mechanical processing [38,39], which correlates well with the behavior of a ternary CuCrZr alloy. Increased concentrations of hafnium have advantages for mechanical strength, less weakening, and better fatigue strength [40–43].

Exothermic precipitation processes of ultra-fine grained (UFG) materials have been analyzed during DSC experiments indicating independent precipitation of mainly Cr-containing and intermetallic CuHf phases [38–40], but the precipitation sequence is not investigated in depth in the literature yet.

To sum up, the gap of CuCrHf alloys processed in industrially applicable manufacturing processes is the main focus of this work [44–46]. Providing a direct comparison of different alloying concepts is of special interest to evaluate the alloys' potential. The properties of materials currently used in the industry should be expanded with a target oriented ternary alloy composition. The scope of the present investigation mainly covers structured analysis to understand the alloying effect of chromium and hafnium in low-alloyed copper alloys and the precipitation process in the case of less intense mechanical treatments prior to aging at moderate temperatures. Afterwards, combined ternary alloys are investigated, contrasted and analyzed in-depth.

2. Materials and Methods

Identically processed alloys CuCr0.7, CuHf0.7, CuCr0.7Hf0.35, CuHf0.7Cr0.35, and CuHf0.7Cr0.7 were the basis of investigations. The 500 g weighing specimens were cast in a gravity die casting process with a VC400 casting machine (Indutherm Blue Power Casting Systems, Walzbachtal, Germany). Raw material Cu-OFE with the individual amount of master alloys (CuHf60 and CuCr10) was melted in a boron nitride-covered graphite crucible and was cast at 1300 °C in a graphite die (5 mm thick bar). Melting and casting were conducted under vacuum conditions. The alloy composition and maximum derivation of 0.05 wt.% from the target composition was proven with a calibrated optical emission spark spectrometer (Spectrotest, SPECTRO Analytical Instruments GmbH, Kleve, Germany). Then, a 120 min solution treatment in a preheated furnace (ME65/13, Helmut ROHDE GmbH, Prutting, Germany) followed by water quenching resulted in a supersaturated solid solution. All steps of heat treatments are visualized in Figure 1. With respect to maximum solubility in copper, CuCr0.7 was annealed at 1000 °C, CuHf0.7 at 960 °C, and ternary alloys at individual temperatures. Therefore, the first experiments analyzed the lowest electrical conductivity after annealing at different temperatures between 1000 °C and 960 °C, guided by metallographic investigations to evaluate the process for the maximum solution. Consequently, CuCr0.7Hf0.35 was heat-treated at 1000 °C, and CuHf0.7Cr0.7 and CuHf0.7Cr0.35 used 970 °C.

Afterwards, some of the binary alloy specimens were cold rolled with a thickness reduction of 25%, 50%, and 75%, respectively, with a deformation ratio of up to $\varphi = 1.4$, using a duo roll stand (0.25 mm equidistant feed rate, roll diameter 110 mm, rotation speed 27 min^{-1}) (Bühler, Pforzheim, Germany). Material processing was generally identical to the related research [6,47–49].

All specimens were then aged up to 24 h at 400 °C or, respectively, 500 °C accompanied by measurements of electrical conductivity with an eddy current test (Sigmascope SMP10, with TF100A for temperature compensation, Helmut Fischer GmbH, Sindelfingen, Germany) and hardness tests with a microhardness tester (HV 0.1) (NEXUS 412A equipped for DIN EN ISO 6507-1:2018 Vickers hardness test, Innovatest GmbH, Selfkant-Heilder, Germany).

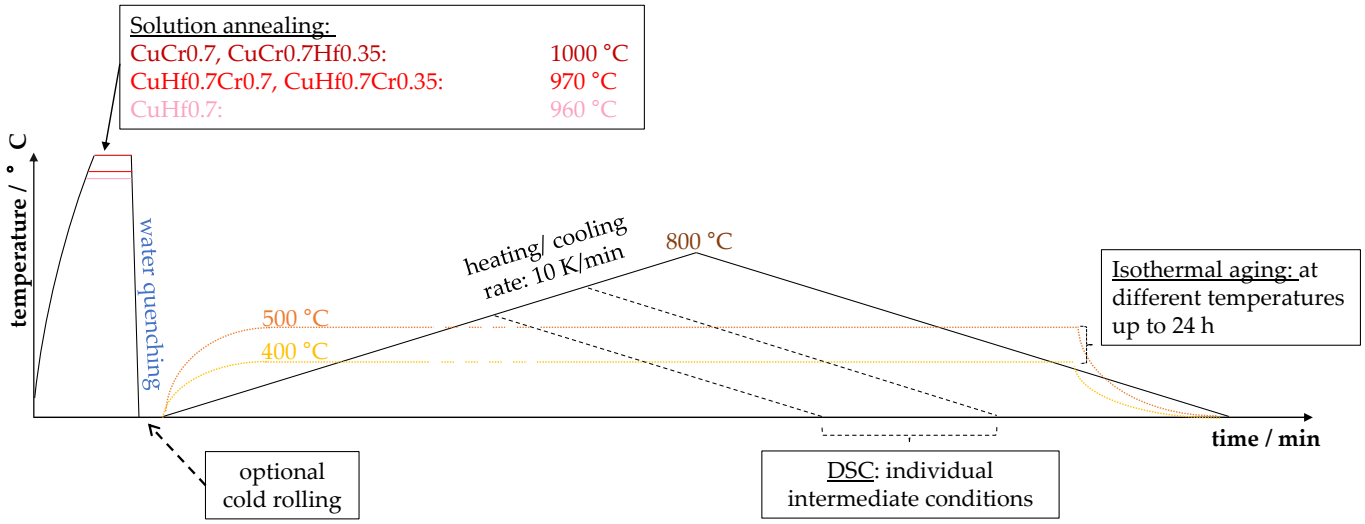

Figure 1. Schematic temperature profile for the production of the copper alloys and the different conducted experiments.

All experimental approaches were supported by metallographic analysis in a scanning electron microscope (Gemini Sigma VP with the used NTS BSD (Carl Zeiss Microscopy Deutschland GmbH, Oberkochen, Germany)).

Following the precipitation process, the differential scanning calorimetry (DSC)-method was utilized (STA 449 F3 Jupiter equipped with a platinum oven for usage up to 1500 °C, NETZSCH-Gerätebau GmbH, Selb, Germany). The solution-annealed and quenched cylindric specimens (117 mg) were heated with a rate of 10 K/min up to 800 °C, where the temperature was held for 1 min, followed by cooling with the same temperature gradient. The heating rate was chosen with respect to mainly used experimental setups for visualizing precipitation processes in aluminum, magnesium, and copper alloys [6,49–52]. A higher heating rate shifts visible exothermic peaks to higher temperatures during the experiment, pointing out the thermally activated and kinetically controlled solid-state reactions [32,35,49]. For metallographic investigations, the experiment was conducted up to a chosen relevant temperature, followed by 1 min of holding and cooling. The atmosphere in the used ceramic crucibles with a lid was argon (50 mL/min), and the measuring device was calibrated with this setup for temperature and enthalpy. The used baseline of each signal was measured multiple times initially and regularly during the experiments with empty crucibles and a Cu-OFE reference during every experiment.

Atom probe tomography (APT) with a LEAP 4000XR device (CAMECA Instruments, Inc., Madison, WI, USA), including laser pulsing equipment and an energy compensating reflectron lens, was utilized to analyze active precipitation processes in-depth. Precise preparation of the specimen tip was mandatory because it needs to be sufficiently sharp to enable the corresponding field emission during APT measurement. For this purpose, multistage electropolishing (10 V followed by 2.5 V with a Struers D2 electrolyte (aqueous solution containing 25–50% phosphoric acid, 15–25% ethanol, and less than 5% propan-1-ol)) was performed. During the gradual evaporation of the specimen at 55 K, position-related flight time was measured for the later reconstruction of the 3D model [53]. The identification of present elements in the specimen was realized by calculating the mass-to-charge ratio of the recognized events due to the impact of accelerated ions on the 2D detector [53]. During the measurements, Cu, Cr, Hf and H were mainly detected (H-ions were present due to impurities in the chamber [54]). A laser pulse with 50 pJ and 250 kHz was used to trigger the field evaporation on the tip. Overall, the detector reached about 37% efficiency. After measurement, reconstruction was performed with Software Ivas 3.6.8 (CAMECA Instruments, Inc., Madison, WI, USA), and further data manipulation and analysis was conducted with the Matlab (The MathWorks, Inc., Portola Valley, CA, USA) APT-toolbox of

P. Felfer [55]. In particular, the present precipitates were of special interest, and rooms of interest (ROI) were added manually in the 3D model to regard the elements' concentration along the z-axis of these areas. In addition, cluster analyses of closed structures in the tip were conducted with the Toolbox of P. Felfer, which adjusts the clustering parameters using Voronoi volumes to the present distribution of atoms [55,56]. Generally, only clusters that were fully within the analyzed volume of the tip were investigated in detail.

3. Results

First, a brief comparison of binary alloys CuCr0.7 and CuHf0.7 highlighted principal differences between the alloying concepts and their precipitation kinetics influencing the macroscopic properties. Aging experiments were used to evaluate hardness and electrical conductivity development for isothermal heat treatments, and DSC measurements characterized exothermic reactions during continuous heating processes. Furthermore, the influence of cold rolling prior to the aging process was compared and discussed for the binary alloys showing that CuHf0.7 was affected much more than CuCr0.7. Choosing different ternary alloys containing chromium and hafnium resulted in the precipitation formation of mainly Cr-containing particles influenced by hafnium atoms as well as intermetallic CuHf phases influenced by the chromium particles. Therefore, precipitation kinetics were highly modified by the presence of the chosen alloying elements and the utilized processing methods.

3.1. Binary Alloys

3.1.1. CuCr0.7

Benchmark alloy CuCr0.7 showed fast precipitation reactions for specimens with and without cold working prior to the aging heat exposure (400 °C and 500 °C). The hardness (Figure 2a) and electrical conductivity (Figure 2b) increased directly within the first hours of aging time for all specimens' treatments.

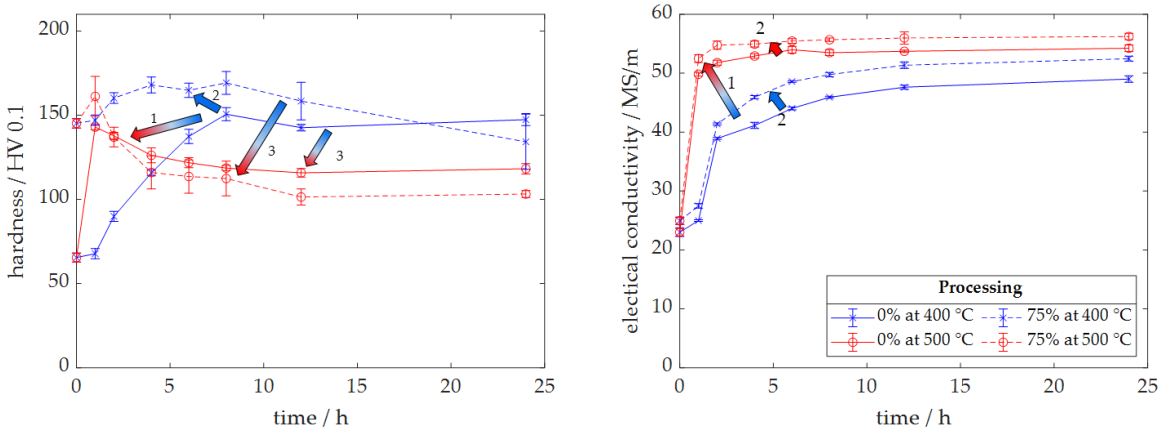

(**a**) (**b**)

Figure 2. Aging heat treatment of CuCr0.7: (**a**) Hardness; (**b**) Electrical conductivity characterizing precipitation process acceleration due to higher aging temperature (1), due to prior cold rolling (75% thickness reduction) (2) and faster overaging at higher aging temperatures (3).

Especially electrical conductivity appeared to be a sensitive parameter for precipitation processes as it increased with the utilized aging temperature (Figure 2b—Arrow 1). With increased temperature, the process was significantly accelerated in the early stages, and maximum values of the macroscopic property were enhanced (Figure 2b) with 49.7 MS/m at 400 °C and 54.5 MS/m at 500 °C aging temperature. Similar effects were visible in the case of pre-deformation (cold rolling with a thickness reduction of 75%). At both investigated aging temperatures, the maximum conductivity was higher for the pre-deformed

specimens (Figure 2b—Arrow 2) with 53.6 MS/m and 56.4 MS/m at 400 °C and 500 °C aging temperatures, respectively.

Regarding hardness, a similar picture can be drawn. Higher aging temperatures significantly accelerated precipitation reactions resulting in hardness increases (Figure 2a—Arrow 1), and pre-deformation shifted the peak hardness to appear earlier as well (Figure 2a—Arrow 2). Cold rolling before heat treatment increased peak hardness at both aging temperatures from 154 HV 0.1 to 169 HV 0.1 (400 °C aging temperature) and 143 HV 0.1 to 161 HV 0.1 (500 °C aging temperature). The maximum hardness showed the benefits of a lowered aging temperature as both specimens (with and without pre-deformation) reached higher values at a 400 °C aging temperature. Furthermore, the higher aging temperature resulted in faster and sharper overaging effects. Especially the cold worked specimen in Figure 2a showed overaging during heat treatment as hardness dropped by about 58 HV 0.1 (500 °C: from peak condition after 1 h to 24 h aging) and 35 HV 0.1 (400 °C: from peak condition after 8 h to 24 h aging) from its peak value.

3.1.2. CuHf0.7

Binary CuHf0.7 showed high potential for precipitation processes as high hardness values were measurable (Figure 3a) with a maximum of 195 HV 0.1 (400 °C for 2 h).

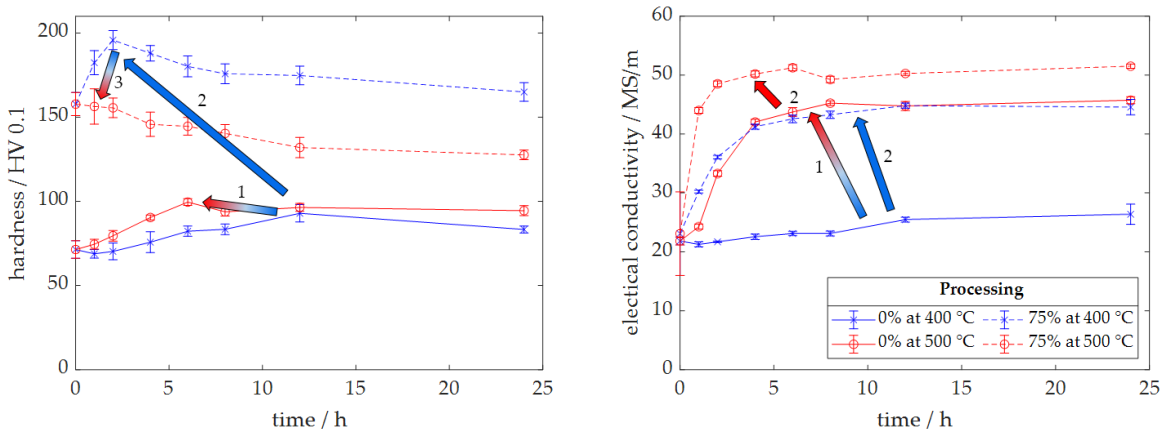

(**a**) (**b**)

Figure 3. Aging heat treatment of CuHf0.7: (**a**) Hardness; (**b**) Electrical conductivity characterizing precipitation process acceleration due to higher aging temperature (1), due to prior cold rolling (75% thickness reduction) (2) and faster overaging at higher aging temperatures (3).

Figure 3a shows how sensitively the alloy reacted to cold rolling prior to an aging process, as the reachable hardness level was mainly affected by this processing. For specimens without pre-deformation, higher aging temperature helped to introduce precipitation reactions and increasing physical properties, characterized by electrical conductivity in Figure 3b. Overall, the cold rolled specimen reached significantly higher electrical conductivities (44.8 MS/m for aging at 400 °C, 51.8 MS/m for aging at 500 °C) compared to the specimen of the directly aged solid solution (32.9 MS/m for aging at 400 °C, 45.9 MS/m for aging at 500 °C); see Figure 3b. The development of electrical conductivity and hardness showed how precipitation processes were accelerated by an increased aging temperature (Figure 3—Arrow 1) and the introduction of pre-deformation (Figure 3—Arrow 2).

Utilizing cold working and the subsequent precipitation reactions resulted in high reachable hardness conditions followed by significant overaging (decrease from a 2 h peak condition to 24 h at 400 °C: 30 HV 0.1), which became even more evident at elevated temperatures (500 °C: 31 HV 0.1); see Figure 3a (Arrow 3). The 500 °C aging temperature combined with the provoked pre-deformed state of the quenched solid solution resulted in declining hardness values directly after 1 h of aging treatment due to the interaction of

hardening mechanisms. For the specimen without cold rolling before aging treatment, no overaging was visible during the applied temperature exposure, but the reachable hardness level was insufficient.

3.1.3. Comparison

Binary CuHf0.7 reacted with a remarkably different characteristic to applied heat treatments than benchmark alloy CuCr0.7.

Overall, alloy CuCr0.7 precipitated fast and showed significant effects referred to heat treatment. A higher aging temperature had a remarkable effect on the alloy as it accelerated the changes in the resulting properties. The hardness increases were significant for all processing options, and high electrical conductivities were reachable. Especially conductivity showed similar results for all processing options, but it appeared to behave sensitively to aging temperature.

The binary CuHf0.7 alloy required more effort for precipitation processes as the sensitive electrical conductivity started to react slower and was highly influenced by prior cold rolling. As mechanical treatment was introduced, the following heat treatment affected the resulting properties faster and more effectively. Whereas 400 °C aging temperature was not enough to reach beneficial properties for the specimen without pre-deformation, 500 °C was too high for the specimen with 75% thickness reduction, and a very fast overaging occurred. On the other hand, CuHf0.7 showed great potential to achieve high mechanical and good electrical properties, particularly noticeable for cold rolled specimens. This potential needs to be further exploited.

3.2. Ternary Alloys

Both alloying concepts, CuCr0.7 and CuHf0.7, highlighted their benefits in binary alloys. In the following, ternary combinations are investigated for specimens directly aged from their quenched solid solution without any influence of pre-deformation.

3.2.1. Hardness and Electrical Conductivity

For an aging treatment at 400 °C, Figure 4 displays resulting properties and visualizes the differences of binary alloys in contrast to several ternary combinations: CuHf0.7Cr0.7, CuHf0.7Cr0.35, and CuCr0.7Hf0.35.

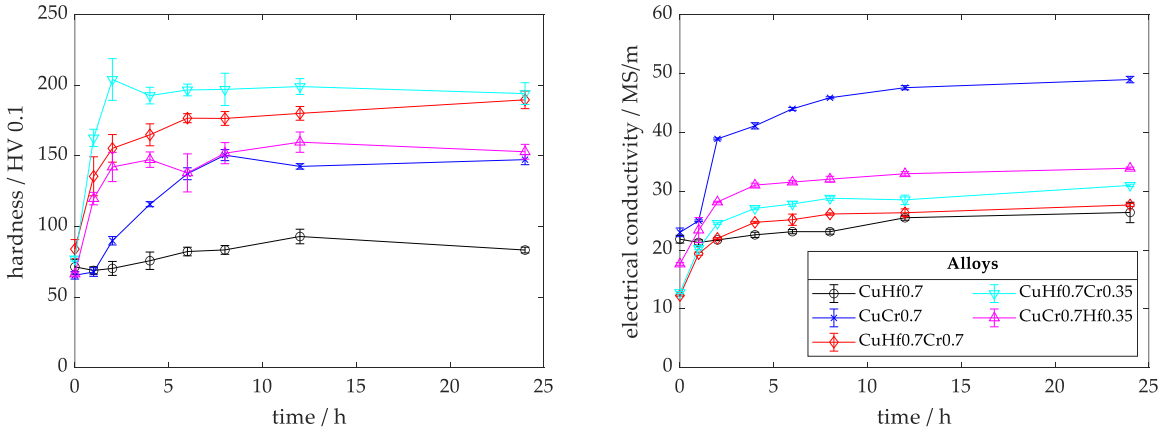

(**a**) (**b**)

Figure 4. Aging heat treatment at 400 °C: (**a**) Hardness; (**b**) Electrical conductivity for the binary and ternary alloys.

Generally, the enhanced alloying content affected the solution annealed condition by slightly increasing hardness (Figure 4a) and significantly lowering electrical conductivity (Figure 4b). These properties were highly modified during the aging treatments.

Alloying CuHf0.7 with chromium dramatically changed the precipitation reaction during heat treatment, directly visible in the resulting hardness (Figure 4a). All ternary alloys followed and further exaggerated the behavior of CuCr0.7 with its fast hardness increase. Reachable peak values were 190 HV 0.1 (CuHf0.7Cr0.7), 204 HV 0.1 (CuHf0.7Cr0.35), and 163 HV 0.1 (CuCr0.7Hf0.35) for the three alloying options. Both alloys with higher hafnium content (CuHf0.7Cr0.7 and CuHf0.7Cr0.35) showed the highest hardness values (Figure 4a) and confirmed the high hardening potential of CuHf0.7.

Regarding electrical conductivity (Figure 4b), higher alloying content resulted in lower conductivities, and CuCr0.7 was the most beneficial option. During the proceeding temperature exposure, electrical conductivity continuously increased for the ternary alloys ending up around 30 MS/m, wherein CuCr0.7Hf0.35 was the best ternary option with a maximum of 37.6 MS/m (Figure 4b).

Aging treatment at an elevated temperature of 500 °C resulted in further enhanced electrical conductivities (Figure 5b). For ternary alloys, the differences between the three options became obviously smaller with 46.1 MS/m (CuHf0.7Cr0.35) to 46.6 MS/m (CuCr0.7Hf0.35) after 24 h of aging. Compared to the binary CuHf0.7, all Cr-containing alloys verified the accelerated property changes due to precipitation processes.

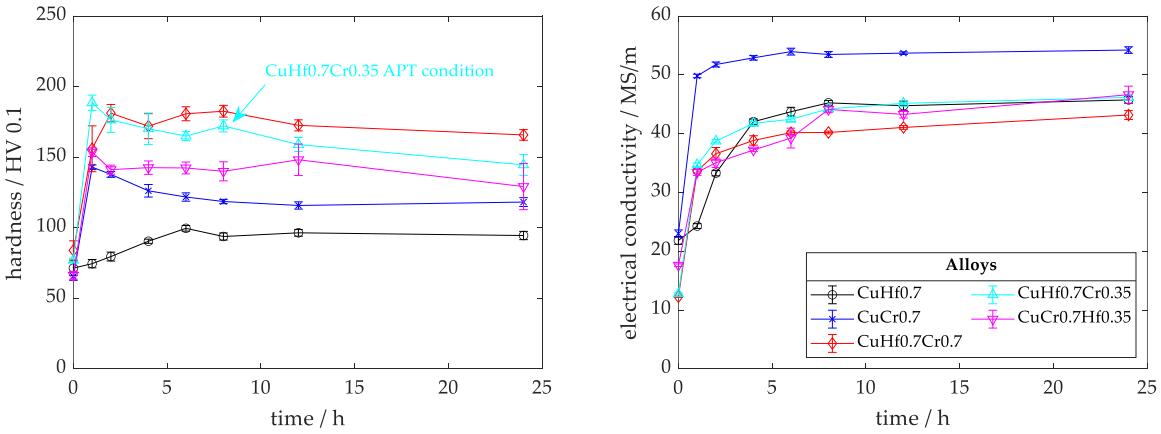

(**a**) (**b**)

Figure 5. Aging heat treatment at 500 °C: (**a**) Hardness; (**b**) Electrical conductivity for the binary and ternary alloys.

Whereas higher temperature was beneficial for the physical properties, hardness (Figure 5a) was significantly influenced by overaging effects. This drop of mechanical properties was a critical disadvantage for binary CuCr0.7, whereas CuHf0.7 did not reach the hardness level of its pre-deformed options. Alloying copper with hafnium and chromium shifted all of these effects in a favorable direction, as the ternary alloys reached high hardness values fast (at this temperature, after 2 h 183 HV 0.1 for CuHf0.7Cr0.7, after 1 h 189 HV 0.1 for CuHf0.7Cr0.35 and after 1 h 154 HV 0.1 for CuCr0.7Hf0.35) in combination with slower and less distinctive overaging (Figure 5a). Whereas hardness sharply dropped for CuCr0.7 after its peak aged condition, the ternary options mitigated this disadvantage at a higher absolute hardness level.

For further in-depth investigations, CuHf0.7Cr0.35 with an aging time of 8 h was defined to display not the early stages of precipitation but a further developed condition to investigate time-dependent interactions between alloying elements and resulting precipitation phases.

3.2.2. Differential Scanning Calorimetry (DSC)

As a next step towards a comprehensive overview of the alloys' precipitation behavior, exothermic peaks related to precipitation reactions were displayed within DSC

measurements. For this comparison, only the options without pre-deformation are shown in Figure 6.

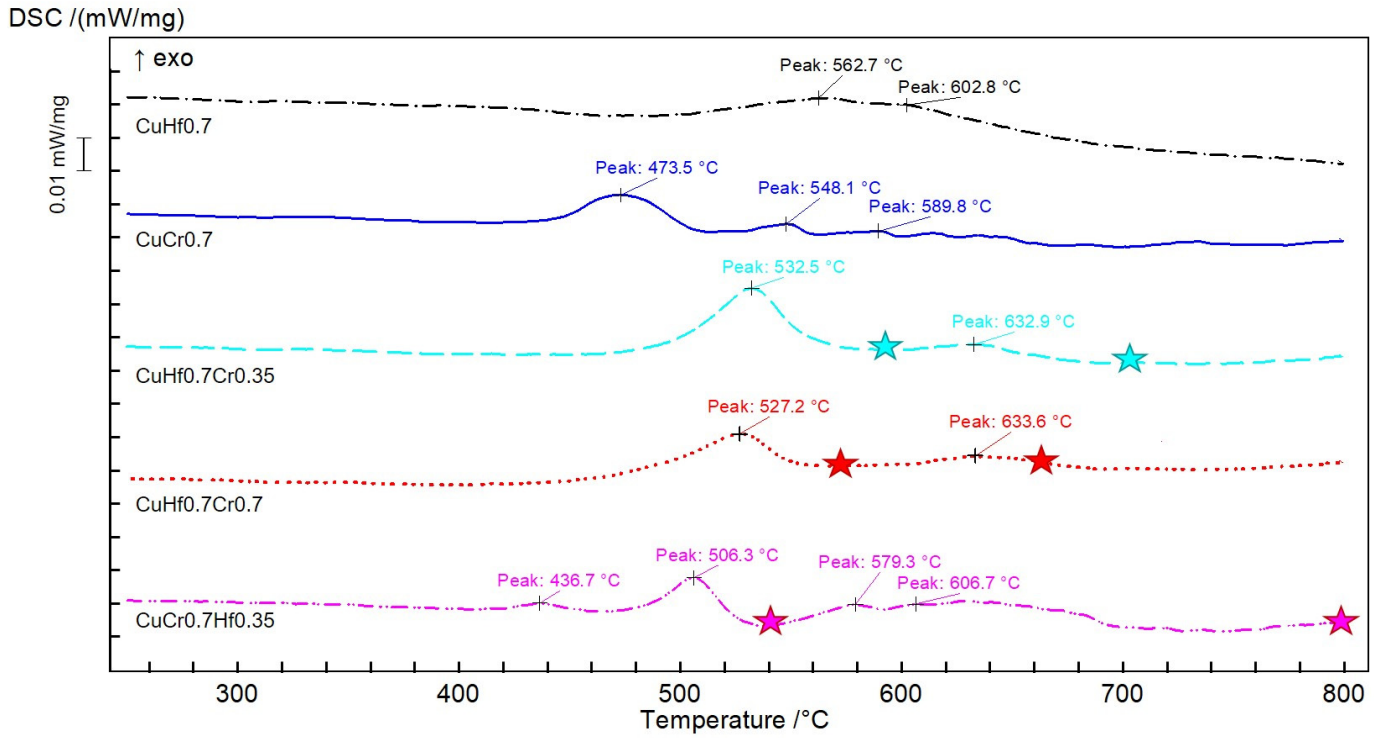

Figure 6. DSC measurement of all binary and ternary alloys without cold rolling prior to the DSC measurement and conditions (stars) for metallographic analysis.

A thorough analysis of the resulting microstructures was conducted to evaluate the interpretation of significant exothermic peaks. Therefore, the experiments were repeated with freshly supersaturated specimens up to the termination of a significant exothermic peak in the DSC profile (marked with a star symbol in Figure 6).

The highest wt.%-ratio of Hf/Cr was observed in CuHf0.7Cr0.35, which characterized the effect of alloying CuHf0.7 with small amounts of chromium. The first visible exothermic peak of the DSC curve shifted to 533 °C, whereas the first visible peak of the binary CuHf0.7 alloy was at 563 °C (Figure 6). With the information of correlating metallographic analysis in Figure 7, this first peak could be evaluated. The brightly contrasted enhanced hafnium concentrations could be referred to intermetallic CuHf phases in Appendix A, Figure A1 utilizing EDS. Furthermore, Figure 7 shows that hafnium atoms tend to migrate into the intergranular space (1) resulting in a precipitate-free zone (4) next to the grain boundary. Within the grains, homogenously distributed precipitates (3) were visible and arranged in some areas on preferred crystallographic planes (2). In conclusion, the first peak of the DSC curve could be related to precipitation reactions with intermetallic CuHf phases. The condition after the first peak showed fine and homogenously distributed precipitates (Figure 7a—Detail 3) within the grains and a slight tendency of these structures to nucleate and grow with preferred orientations (superordinate visible line structures in Figure 7a—Detail 2). Furthermore, a second peak appeared for the ternary alloy at 633 °C, which was after the exothermic effects of binary options (Figure 6). The corresponding metallographic analysis after heating up to 700 °C (Figure 7b) showed coarsening of the already known precipitates. With identical magnification, the visual impression fitted to the trend of growing and coarsening precipitates (Figure 7b—detail 5) as some of them were already in a rod-like shape (Figure 7b—detail 6) and seemed to disappear at the expense of fine earlier-stage precipitates (Figure 7a—Detail 3). Corresponding to the EDS analysis of

Appendix A, Figure A1, no further statement about accumulations of chromium could be made at this point.

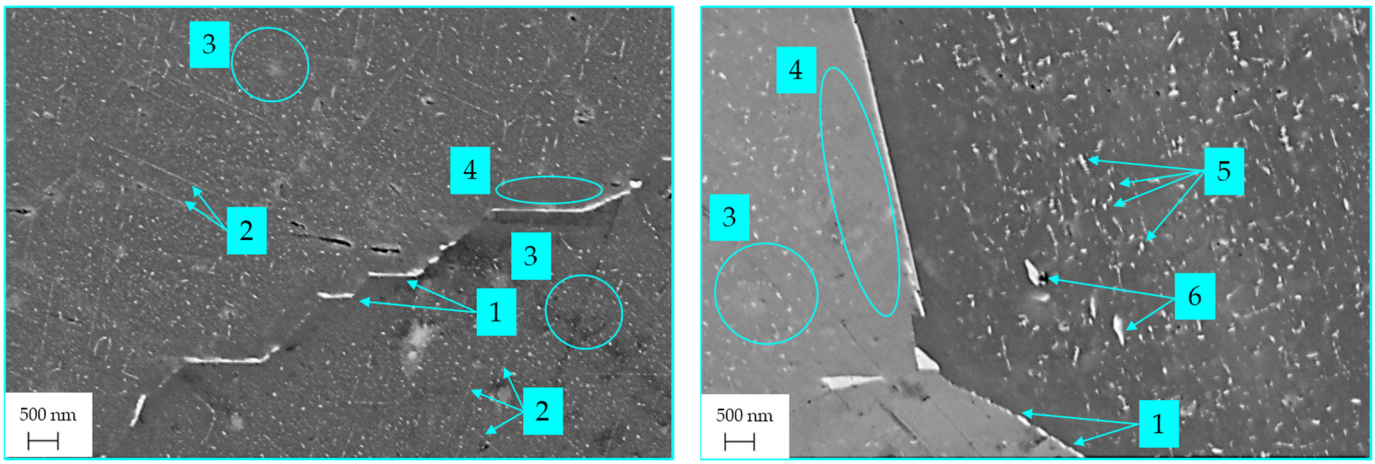

(**a**) (**b**)

Figure 7. CuHf0.7Cr0.35 microstructure evolution during DSC measurement: (**a**) Heating up to 590 °C; (**b**) Heating up to 700 °C with intermetallic CuHf phases in the intergranular space (1), intermetallic precipitates with preferred crystallographic planes for nucleation (2), finely distributed intermetallic CuHf precipitates (3), less Hf concentration next to grain boundaries (4), coarsened intermetallic CuHf precipitates (5) and ripened intermetallic CuHf phases in a rod-like shape (6).

With an enhanced alloying content of chromium, CuHf0.7Cr0.7 continued this trend of the previously analyzed CuHf0.7Cr0.35 alloy. The first exothermic reaction occurred at 527 °C, which was only slightly shifted (5 K) to lower temperatures (compared to CuHf0.7Cr0.35). The second occurring peak remained nearly constant at 634 °C and showed a lower dependency on the higher alloying content. In this context, the metallographic analysis of Figure 8 fitted the underlying trend and showed a slightly further intensification of the observed effects at CuHf0.7Cr0.35. A lot of homogenously distributed CuHf precipitates became visible within the grains (Figure 8a—detail 3), and due to hafnium atoms migrating into the intergranular space (Figure 8a—detail 2), a Hf-depleted area was visible next to the grain boundary (Figure 8a—detail 4). Because of the higher alloying content in this option, some as-cast Cr-containing particles were visible in the grains or at grain boundaries. Hf-containing phases grew at such phase boundaries during aging treatments (Figure 8a—Detail 1). Heating up to 660 °C after ending the second exothermic peak of this alloy in the DSC signal of Figure 6 resulted in coarsening precipitates (Figure 8b—Detail 5) and ripening to rod-like morphologies (Figure 8b—detail 6). Resolving Cr-containing precipitates with EDS analysis was impossible. Based on the ways in which chromium as-cast phases appear in the BSD contrast, some ripened Cr-containing precipitates could be visible after extended heat treatment (Figure 8b—Detail 7).

Further decreasing of the wt.%-based ratio of Hf/Cr lead to the CuCr0.7Hf0.35 alloy. Regarding the DSC signal in Figure 6, several characteristics of the binary CuCr0.7 alloy became obvious. After a minor early exothermic reaction with peak temperature at 437 °C, a further reaction at 506 °C followed, and another effect with stretched temperature area covering several sub-peaks (579 °C and 607 °C) affiliated. In direct contrast to the DSC signal of binary alloys, both characteristics of CuCr0.7 with its scattering multiple peaks and the stretched exothermic effect of CuHf0.7 reflected within the DSC signal of CuCr0.7Hf0.35. Further metallographic investigations followed for heating up to 540 °C and 800 °C (Figure 9) to contextualize the exothermic reactions. As shown in Figure 9a—Detail 1, only some undissolved chromium as-cast phases, sometimes attached by hafnium phases, were detected. It was impossible to gain information on Cr- or Hf-

containing phases in this temperature range, neither with the highly contrasting BSD detector, nor the utilized EDS detectors.

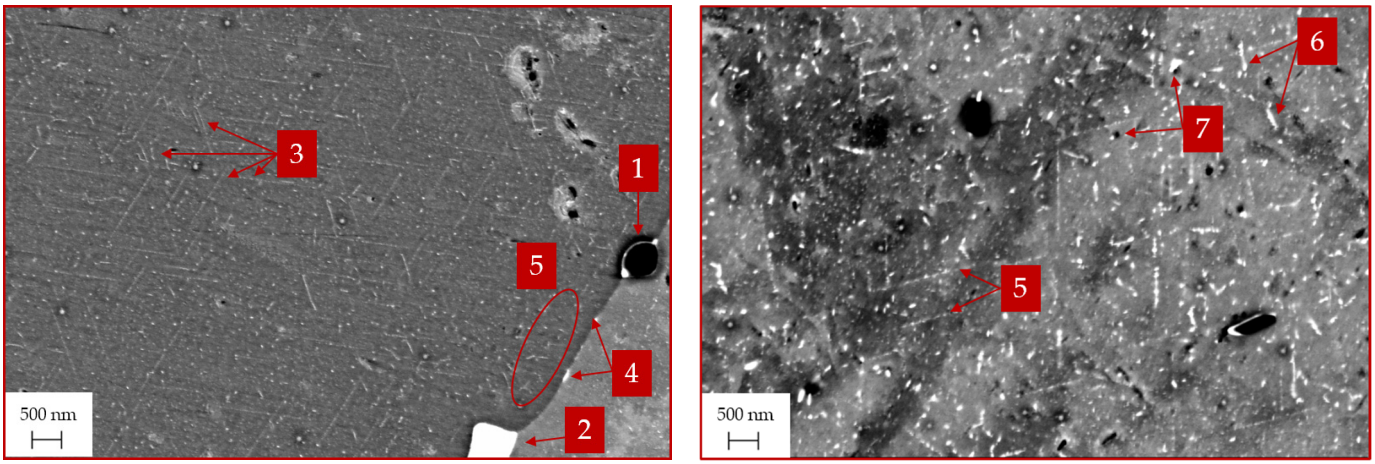

(**a**) (**b**)

Figure 8. CuHf0.7Cr0.7 microstructure evolution during DSC measurement: (**a**) Heating up to 570 °C; (**b**) Heating up to 660 °C with chromium as-cast phases attached by a CuHf phase (1), Intermetallic CuHf phases grew in the intergranular space because Hf atoms tended to migrate there (2) which resulted, compared to the homogenously distributed CuHf precipitates (3), in a reduced density of CuHf precipitates in the grain next to the boundary (4). Later, CuHf precipitates coarsened (5), ripened in needle-shaped intermetallic CuHf phases (6), and intermetallic coarsened CuHf phases next to a coarsened Cr-containing particle became visible (7).

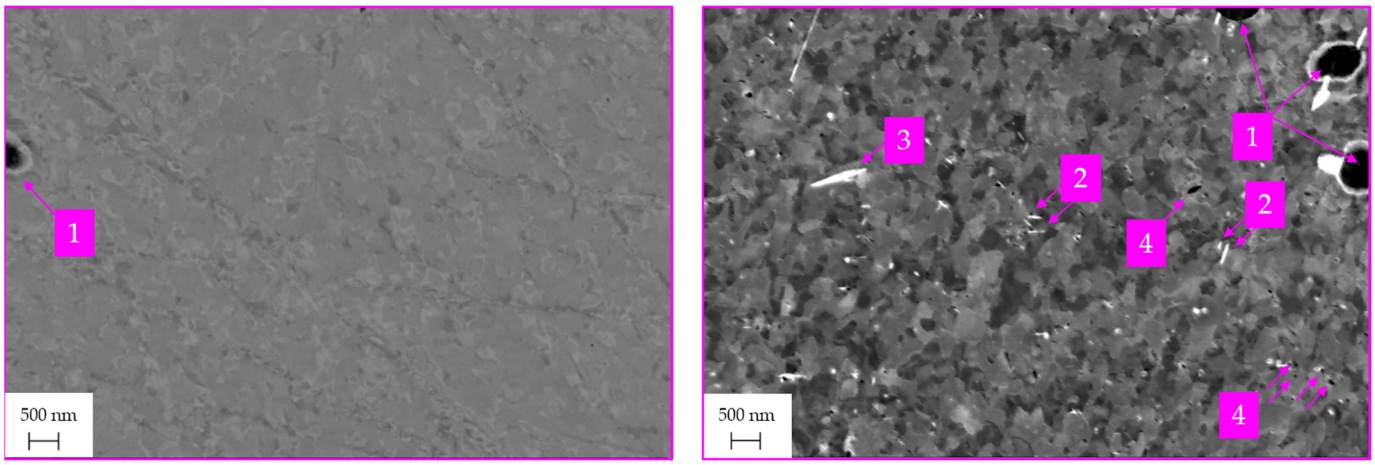

(**a**) (**b**)

Figure 9. CuCr0.7Hf0.35 microstructure evolution during DSC measurement: (**a**) Heating up to 540 °C; (**b**) Heating up to 800 °C showing undissolved chromium phases within a grain (1), coarsened intermetallic CuHf precipitates (2), ripened intermetallic CuHf needles (3) and coarsened Cr-containing precipitates (4).

Further heating up to 800 °C exaggerated place-taking effects for metallographic investigations in Figure 9b, where some coarsened intermetallic CuHf precipitates (Figure 9b—Detail 2) and ripened rod-like Hf-containing needles (Figure 9b—Detail 3) were visible with bright contrast. Contextualizing the dark contrasted phases, known as Cr-containing particles, enabled investigating smaller dark elliptic structures (Figure 9b—Detail 4) and referring them to coarsened Cr-containing precipitates.

To sum up, a structured discussion of precipitation processes helped to draw a consistent picture of place-taking effects during temperature treatment. Nevertheless, further

in-depth investigations were necessary to analyze the essential phenomena and interactions of hafnium and chromium in ternary alloys to understand and contextualize the resulting beneficial properties of these alloys.

3.2.3. Atom Probe Tomography (APT)

For in-depth investigation of precipitation mechanisms, CuHf0.7Cr0.35 was aged for 8 h at 500 °C. For optimum probability to show different stages of precipitation, a slightly overaged condition was chosen (refer to Figure 5). The first metallographic overview of this condition showed that fine intermetallic Hf-containing phases, with their bright BSD contrast, were homogeneously distributed in the grains (Figure 10—Detail 2) of CuHf0.7Cr0.35. Due to the migration of hafnium atoms to the intergranular space (Figure 10—Detail 1), the region next to the grain boundary revealed a reduced amount of these structures (Figure 10—Detail 4). Furthermore, in local effects, the precipitates tended to nucleate on preferred crystallographic planes (Figure 10—Detail 3), resulting in visible ordered elongated structures.

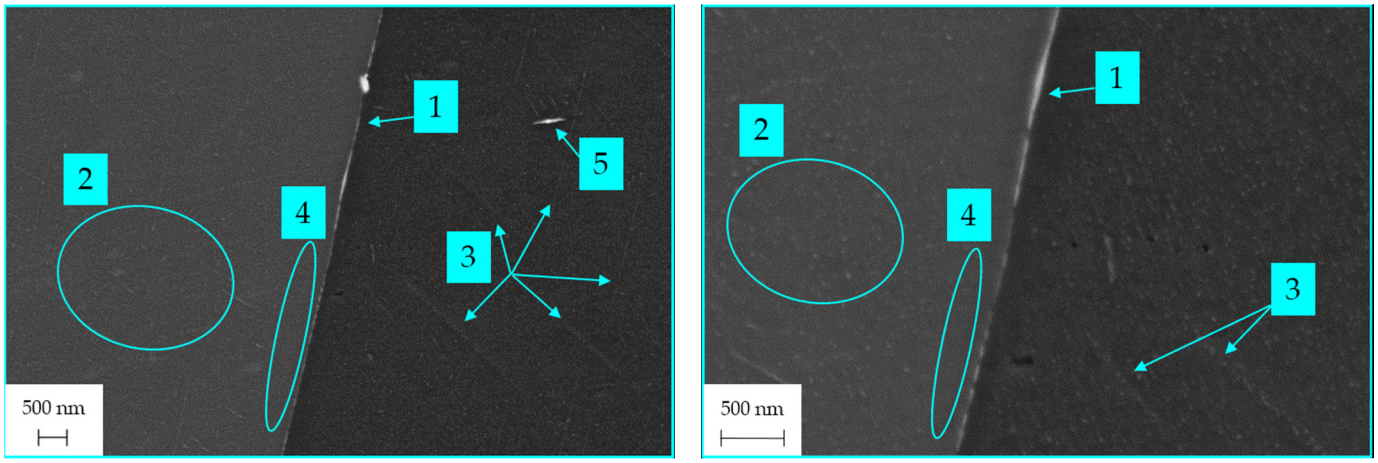

(**a**) (**b**)

Figure 10. CuHf0.7Cr0.35 microstructure after 8 h at 500 °C: (**a**) Overview; (**b**) Detail with hafnium migrating to the intergranular space (1), fine and homogenously distributed intermetallic CuHf precipitates (2), which locally tend to orientate on preferred crystallographic planes for nucleation (3) and a reduced amount of intermetallic CuHf precipitates next to a grain boundary (4) as well as next to a coarsened Hf-containing needle (5).

APT investigations were conducted in this condition to extend the knowledge of these precipitating structures in CuHf0.7Cr0.35. Figure 11 visualizes the results of this measurement with all hafnium and chromium atoms inserted and only 10,000 copper atoms were not hidden (overall, the measurement included about seven million atoms). Furthermore, Figures 12 and 13 refer to this measurement and the documented rooms of interest (ROI).

In Figure 11, it is directly visible that CuHf structures were persistently localized next to precipitates with high chromium content. Figure 12b illustrates the result of calculations on five chromium clusters with a slightly elliptic shape. The size of these structures was about 8 nm to 13 nm with an average volume of 290 nm^3. These precipitates in the lower nanometer scale were finely and homogenously distributed in the material. Comparing different accumulation of precipitates offers the opportunity to follow the attachment of hafnium atoms to the interface between the Cr-containing precipitate and the copper matrix during the following aging treatment (Figure 12a). With further accumulation of hafnium atoms, independent Hf-containing precipitates nucleated and grew, and their morphology developed in an elongated shape (Figure 12a). For example, as shown in Figure 11, the

upper and largest intermetallic CuHf precipitate had its origin of growth on the surface of the precipitate with high chromium concentration.

Overall, the copper matrix (without the clustered precipitates) appeared to be mainly free of solute alloying atoms (only 0.13 at.% were still measured, Figure 12b).

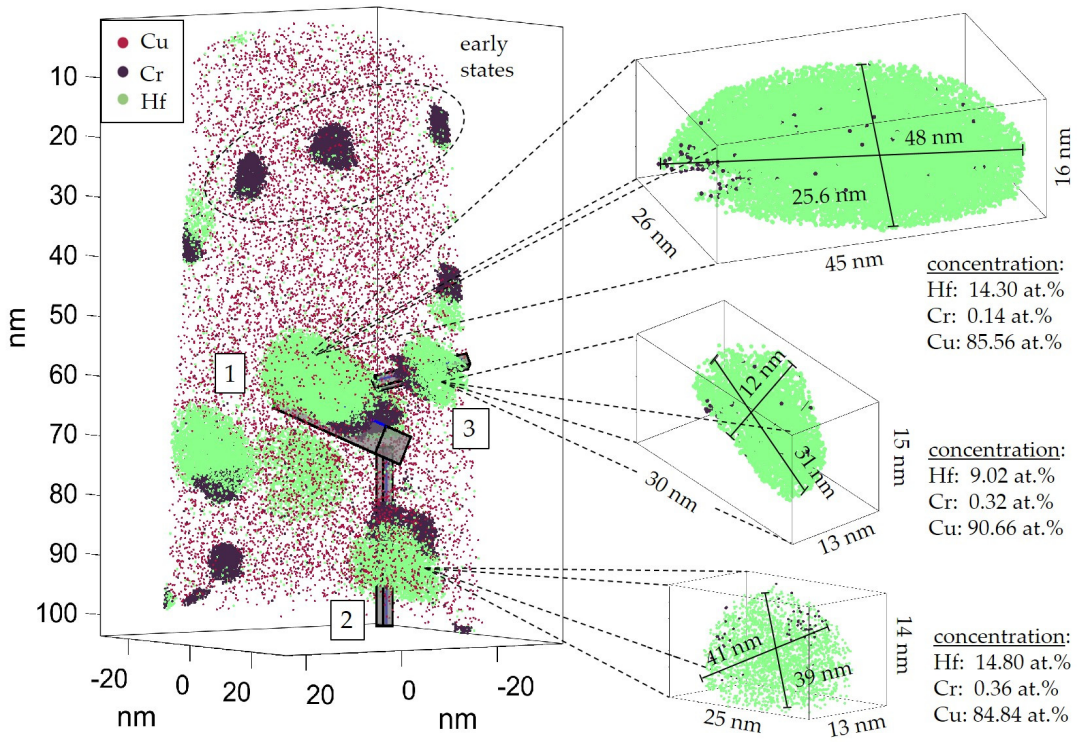

Figure 11. Three-dimensional atom maps of CuHf0.7Cr0.35 after 8 h aging at 500 °C with 10,000 Cu and all measured Cr and Hf atoms displayed. Overview of the specimen with three inserted ROI and cluster analysis of three intermetallic CuHf precipitates. The tree-dimensional visualization is supported by the Video S1.

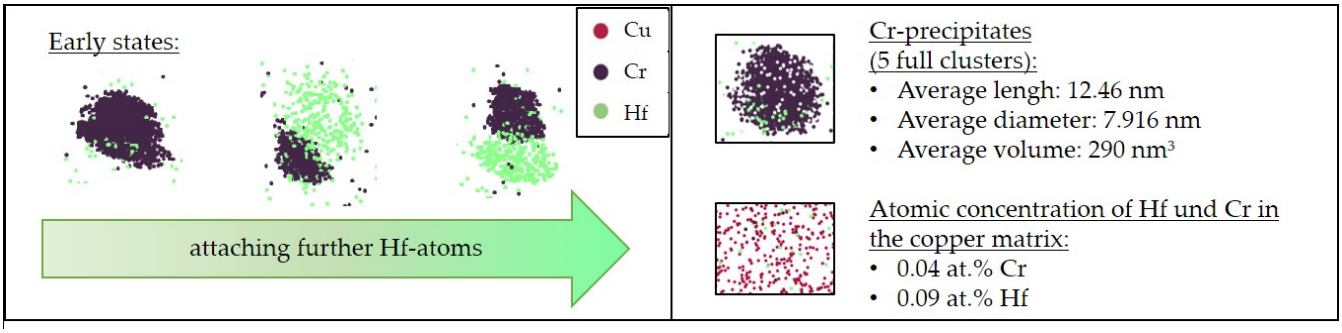

(**a**) (**b**)

Figure 12. Details of results from APT measurement: Evolution of growing intermetallic CuHf next to Cr-containing precipitates with the continuous attachment of hafnium atoms (**a**). Analysis of atomic concentrations in clusters referred to Cr-containing phases and the copper matrix (**b**).

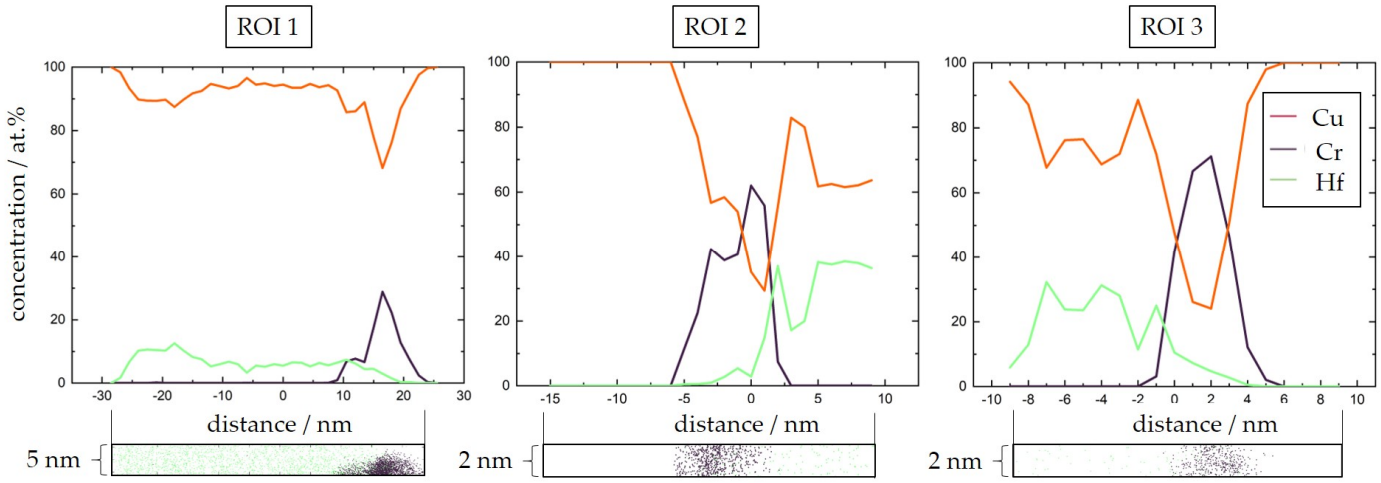

Figure 13. Concentration profiles along the ROI referring to the APT measurement overview of Figure 11 including the visualization of the Cr and Hf atoms within the ROI.

Furthermore, Figure 11 illustrates the three investigated ROI which cover a mainly Cr-containing and an CuHf precipitate each. Figure 13 visualizes the corresponding 1D concentration profile plots.

Within concentration profiles of Figure 13, the concentration of chromium atoms in the referred precipitate was comparably high, with a significant drop of copper concentration in this area, which could be related to a mainly Cr-containing phase. Following the concentration profile to the interface of this small precipitate, a fluent transition to the Hf-containing phase followed within two to five nanometers. The concentration profiles suggested concentrations between 18 at.% and 38 at.% Hf in these phases, which did not enable identification of precipitate composition. Further approach was the analysis of present atoms within the clustered shell. Both of the precipitate next to ROI 1 and that next to ROI 2 showed concentrations of about 14.5 at.% Hf. The third and smallest precipitate of APT measurement (12 nm thickness and 31 nm length) next to ROI 3 contained 9.0 at.% Hf.

4. Discussion

Following the scientific path from binary alloys containing chromium and hafnium, with CuCr0.7 representing the industrial benchmark alloy, guided from the impact of pre-deformation and following aging heat treatments to utilizing ternary alloy concepts and in-depth investigations of precipitation effects.

4.1. Discussion of Binary Concepts and the General Utilization of Prior Cold Rolling

CuHf0.7 reached higher hardness values than CuCr0.7, underlining its potential for low-alloyed copper alloys with high mechanical properties. Disadvantages of CuHf0.7 were slow precipitation reactions and the necessity of pre-deformation by cold rolling for sufficient precipitation reactions. Numerous crystallographic defects and potential precipitation sites were beneficial for this alloy. Overall, the cold rolled CuHf0.7 specimen reached higher electrical conductivities than the directly aged solid solution specimen (Figure 3b). As the electrical conductivity is very sensitive towards solute alloying elements in the matrix metal, this property can be transferred to place-taking precipitation processes and to the precipitated volume fraction. Conduction electrons are scattered at solute elements in the copper matrix and less influenced by precipitates as conductivity increases with the continuing dissolution of alloying elements. This matches the known effects [2,17,57,58].

Generally, CuCr0.7 did not show the need for pre-deformation by cold rolling to enable favorable outcomes during precipitation reactions (Figure 2), which helps this alloy concept to be easily adjustable for industrial applications.

Due to hafnium's comparatively large atomic radius, its diffusion in the copper lattice is more difficult, which results in the need for elevated temperatures (Figure 3) to introduce precipitation reactions [2]. Paths of facilitated diffusion along the core of dislocations [4,59] strongly promote the mobility of hafnium atoms in the surrounding copper matrix. Cold rolling significantly increased the density of dislocations, resulting in the measured properties. In contrast, chromium atoms can move more easily because of a similar atomic radius to that of copper.

4.2. DSC Investigations with Binary Alloys Containing Hafnium or Chromium

DSC analysis underlined the investigated results of properties and concluded with a coherent picture. Compared to the CuCr0.7 alloy, CuHf0.7 presented its exothermic DSC precipitation reactions about 90 K higher. For CuHf0.7, the precipitation of Cu_5Hf and the following solid-state reaction to $Cu_{51}Hf_{14}$ [25] blurred in one effect at the chosen heating rate [6]. For CuCr0.7, multiple exothermic effects followed the first outstanding exothermic reaction. Due to the processing of these specimens, only temperature–time-dependent solid-state reactions related to the precipitation process needed to be considered [6].

Generally, good comparability to the already discussed temperatures of the benchmark alloys was given. For a quenched solid solution of CuCr0.8Zr0.08, Dalan et al. [59] reported an exothermic peak at 441 °C after solution annealing at 1020 °C and 493 °C after solution annealing at 930 °C utilizing a comparable heating rate. During the measurement of the present study, the binary CuCr0.7 showed a peak temperature of 468 °C after solution annealing at 1000 °C, which underlines high comparability.

4.3. DSC Investigations with Ternary Alloys Containing Hafnium and Chromium

Alloying CuHf0.7 with small amounts of chromium (CuHf0.7Cr0.35) helps to significantly shift these exothermic peaks about 30 K to lower temperatures (Figure 6). A further increased chromium content (CuHf0.7Cr0.7) continues this trend slightly accelerating precipitation reactions. The first huge exothermic effect, related to the precipitation formation and first growth in CuHf0.7Cr0.35, was further shifted by 5 K to lower temperatures due to the higher chromium content in CuHf0.7Cr0.7, increasing the supersaturation and driving force for precipitation reaction. This demonstrates that CuHf0.7Cr0.35 fully utilizes its potential in terms of precipitation kinetics. In the context of the DSC signals related to CuCr0.7 and CuHf0.7 (Figure 6), the first exothermic effects of CuHf0.7Cr0.35 were likely related to solid-state reactions with chromium and accelerated reactions of hafnium, which were approved by the metallographic investigations of Figures 7 and 8. Consequently, this behavior fits very well with the experience from the measurements of hardness and conductivity (Figures 4 and 5).

The second type of investigated exothermic DSC effects with less energy release, related to a visible coarsening of precipitates in both alloys (CuHf0.7Cr0.35 and CuHf0.7Cr0.7) which could include further changes in precipitation structures, stayed nearly at the same temperature during DSC measurement. Therefore, these processes were not influenced by an elevated chromium content.

In direct comparison with DSC measurements carried out by Bochvar et al. (CuHf0.9Cr0.7) [44], parallels to the experiments conducted in this work with the same heating rate can be observed. Bochvar et al. [44] showed only the temperature range up to 600 °C. In the low-temperature range, Bochvar et al. observed only one exothermic effect with peak temperature at 560 °C, which can be correlated to the first exothermic effect at 527 °C in this work. The differences could be explained by the chosen annealing temperature. Bochvar et al. carried out solution annealing at lower temperatures resulting in a lower supersaturation compared to the materials in this work. Furthermore, the exothermic DSC effect of Bochvar et al. showed a sub-peak in the rising flank, which was not visible in the present experiments. Based on the generated knowledge, this could be related to early precipitation of Cr-containing precipitates as well, which were not visualized yet.

4.4. APT with CuHf0.7Cr0.35

To investigate the active effects during precipitation processes in ternary alloys, APT was a key factor to show how intermetallic CuHf structures are localized next to Cr-containing precipitates (Figure 11). For geometrical comparison, Figure 12 shows good correlation of the investigated clusters of mainly chromium and their known coffee been shape [11] with a matching dimension (5 nm to 10 nm) to that of already investigated sizes [11,12,14].

During aging heat treatment, hafnium atoms attached to the interface of the homogenously distributed mainly Cr-containing precipitates and started to nucleate and grow there to intermetallic phases with elongated morphology (Figure 12).

Here, the investigation of three ROI, which covered one of the precipitate specimens each, revealed the corresponding integral profile of concentrations (Figure 13). Within the Cr-containing precipitates, the concentration of chromium atoms was comparably high, with a significant drop in the copper concentration, which could be related to the formation of precipitates of mainly chromium [11,12,14]. Following the concentration profile to the interface, a fluent transition to the Hf-containing phase became obvious within two to five nanometers. The concentration profiles suggested concentrations between 18 at.% and 38 at.% Hf in these intermetallic structures. The identification of the concrete composition was not possible at this stage. Further approach was the analysis of atoms within the clustered shells. Both of the precipitates next to ROI 1 and ROI 2 showed concentrations of about 14.5 at.% Hf. Direct relation to the possible intermetallic structures for these precipitates, with 16.7 at.% for the Cu_5Hf and 21.5 at.% for the $Cu_{51}Hf_{14}$, was not easily possible. The third precipitate next to ROI 3 contained 9.0 at.% Hf. Direct comparison to the critical precipitate radius for this transition at 9.5 nm of Jiang et al. (binary CuHf alloy) can provide further clues [25]. For the smallest precipitate of the APT measurement in this work (12 nm thickness and 31 nm length), a reduced hafnium content was measurable. In this size range, phase transformation could be realistic in case of the present crystallographic structure with its inherent defects. Therefore, it could be indicated that precipitation structures of both Cu_5Hf and $Cu_{51}Hf_{14}$ were present (suggesting a deviation of about 7.5 at.% for the clustered hafnium concentrations that could fit the early-stage precipitate of Cu_5Hf for ROI 3, whereas the two others could fit the $Cu_{51}Hf_{14}$ phase) but could not be finally identified for ROIs 1 to 3. At this point, further investigations to identify the crystallographic structure are necessary. In-depth investigations with TEM on the microstructure and distribution of shown precipitates will expand the knowledge on these temperature–time-dependent processes.

Within the interface between the mainly Cr-containing particle and the copper matrix, hafnium atoms obtain a favorable site to segregate and to reduce elastic distortion energy. By accumulating in this local area, the further growth of these precipitates is possibly hampered, which would correlate with the known and commonly used in the industry effect of zirconium atoms in CuCr1Zr [22,24]. Due to the already increased hafnium concentration next to the interface, more hafnium atoms attach, and the barrier for nucleating the referring precipitate is reduced. Therefore, the Hf-containing precipitates saddled at the site of the existing Cr-containing phases within the conducted experiments. Due to the homogenously distributed nanoscale mainly Cr-containing precipitates, a considerable offer of potential nucleation sites for the Hf-containing precipitates was introduced in the material. Many small intermetallic CuHf precipitates were evolving at the same time. Therefore, target-oriented usage and fast introduction of the materials' high hardening potential was possible as summarized in Figure 14. To sum up, mainly Cr-containing precipitates were utilized as catalysts for the following precipitation reactions of finely distributed and highly strengthening intermetallic CuHf precipitates. Furthermore, the accumulation of hafnium atoms next to Cr-containing precipitates could hamper their growth and contribute to reduced overaging during isothermal aging experiments.

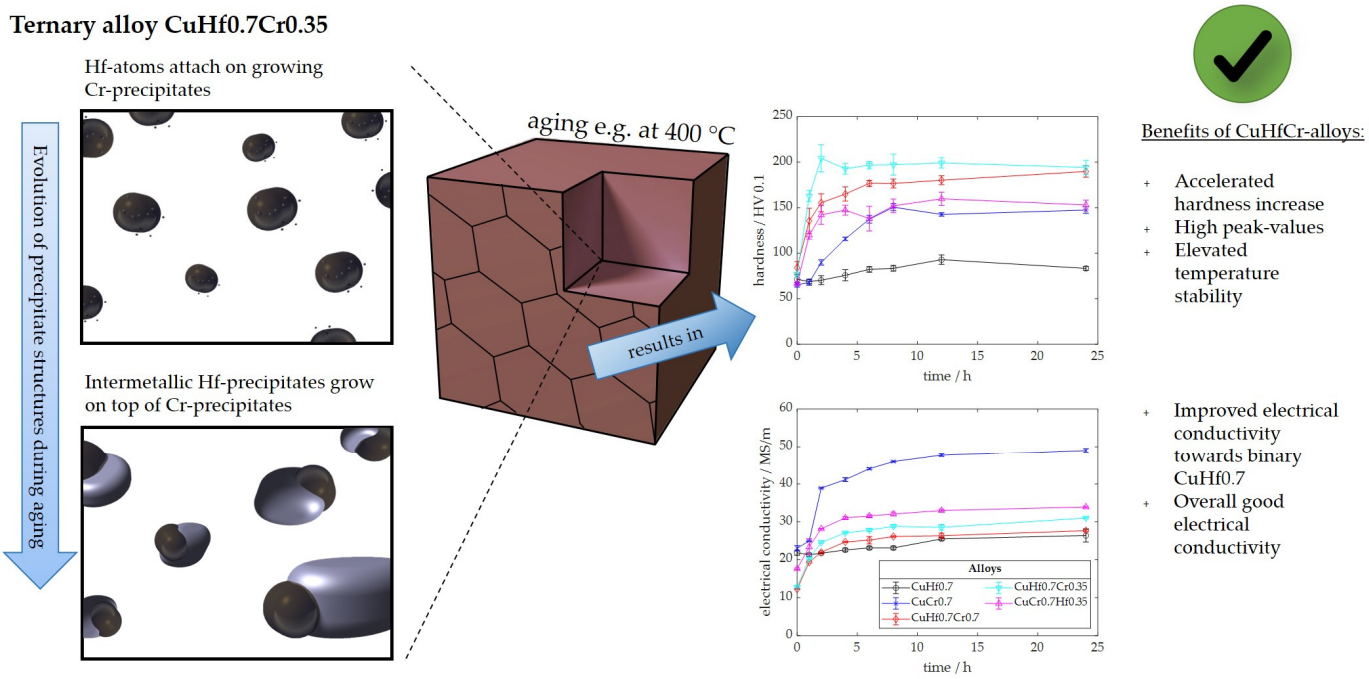

Figure 14. Summary of the schematic aging process of CuHf0.7Cr0.35 with early chromium precipitates, attaching hafnium atoms and intermetallic CuHf precipitates saddling on top of chromium precipitates. The precipitating phases contribute to beneficial material properties during aging at an exemplary temperature of 400 °C.

4.5. Perspectives of Ternary Copper Alloys Containing Hafnium and Chromium

Overall, the copper matrix appeared to be mainly free of solute alloying elements, which directly fits the behavior of electrical conductivity as a sensitive parameter for solute foreign atoms. Whereas the evolution from the initial supersaturated quenched condition to the aged condition after 8 h at 500 °C gained 31.55 MS/m, further aging could only slightly continue this trend (Figure 5b). Finding an optimal compromise for further application-related research activities needs a closer discussion of characterizing properties regarding all discussed ternary alloys. For the analyzed hardness and electrical conductivity, CuHf0.7Cr0.35 provided an excellent combination of properties (maximum hardness of 204 HV 0.1, 33.2 MS/m and only about 14 HV 0.1 overaging (Figure 4)). CuHf0.7Cr0.7 increased the hardness slightly, but this benefit is paid for with reduced electrical conductivity. Furthermore, the conducted experiments showed that CuCr0.7Hf0.35 lacks peak hardness compared to the other concepts and only provided some improvement for less overaging (Figures 4 and 5). Optimizing an individually adjusted heat treatment routine needs further discussion of different combinations for temperature and time of the utilized heat treatment and will be performed in the near future.

Nevertheless, ternary alloys with hafnium and chromium showed their huge hardening potential without the need of pre-deformation by cold rolling, which was beneficial compared to the binary CuHf alloy. Their accelerated precipitation reactions reduced the need for energy-consuming heat treatments and were applicable without prior mechanical treatments. This helps industrial usage with an easy adjustment of properties in different shapes and conditions of the material. Compared to the benchmark alloy containing mainly chromium, represented by CuCr0.7, elevated mechanical properties and less overaging were reachable.

Finally, one possible field of application for these alloys is the manufacturing technology in mechanical and automotive engineering. For example, electrode tips for resistance spot welding can profit from these mechanically durable materials with elevated thermal and electrical conductivity [60–62]. In electrical engineering, their use as a contact material

in connectors, contacts, and switches would be particularly target-oriented [63–65]. Further fields for high-performance copper alloys are, for instance, rocket combustion chambers.

Powder bed-based additive manufacturing processes are industrially relevant processes for prototype and small series production. So far, the processing of pure copper, as well as various alloys such as CuCr1Zr, CuNi2.5SiCr, CuNi30Mn1Fe, NiCu30Fe [66], or CuSn11 [67] has mainly been investigated. Subsequent heat treatment increased the electrical conductivity [68,69] and mechanical properties [70] of precipitable copper alloys such as CuCrZr and CuNiSi in the additive manufactured condition. For propulsion applications in space, temperature-stable alloys with chromium and niobium are relevant [71,72], and the ITER project uses CuCr1Zr in additive processing as well [73]. Small heat exchangers, thermal elements, or components in the electronic industry could profit. In this context, heat treatment at moderate temperatures is desirable to minimize warpage [68,74]. Alloys with hafnium and chromium appear to have a beneficial advantage for additive manufacturing processes because they utilize effective precipitation reactions without prior cold rolling. The achievable mechanical material properties will exceed those of the CuCrZr alloys.

5. Conclusions

Thermal and mechanical treatment and target-oriented alloying conceptualization influenced precipitation processes in supersaturated solid solutions of copper alloys with chromium and hafnium. The conglomerate of different approaches to understanding present precipitation mechanisms can be summarized.

1. Binary copper alloys with low hafnium concentration needed diffusion-facilitating influences to promote following precipitation reactions due to hafnium's larger atom radius and therefore lowered diffusivity. Cold working prior to aging treatment introduced paths of higher diffusion, which became visible in peak shifts of conducted DSC measurements and reflected in resulting material properties such as hardness and electrical conductivity.
2. Electrical conductivity reacted very sensitively regarding solute atoms in the copper matrix and increased significantly within place-taking precipitation processes of the supersaturated quenched metals. In direct comparison, CuCr0.7 had the highest electrical conductivity with maximum 49.7 MS/m and 53.6 MS/m after 24 h of aging at 400 °C (without and with 75% thickness reduction by cold rolling), whereas CuHf0.7 reached only 26.4 MS/m and 44.8 MS/m. Ternary alloys aged without cold rolling reached, in the case of CuHf0.7Cr0.7, 28.7 MS/m, and in the case of CuHf0.7Cr0.35, it was 31.0 MS/m.
3. Regarding hardness, the ternary alloys significantly expanded the range of mechanical properties and appeared to be beneficial in comparison to binary alloys. Best hardness values without cold rolling prior to the aging process were obtained at 400 °C aging temperature with CuHf0.7Cr0.35 (204 HV 0.1) and CuHf0.7Cr0.7 (194 HV 0.1), whereas binary alloys such as CuCr0.7 reached only 154 HV 0.1. In the case of aged binary alloys cold rolling with 75% thickness reduction increased the reachable peak hardness at this aging temperature to 169 HV 0.1 (CuCr0.7) and 195 HV 0.1 (CuHf0.7). Ternary alloys showed beneficial hardening potential with accelerated reactions without the need of prior cold rolling.
4. Precipitates containing mainly chromium were visible in the ternary CuHfCr alloys. During the conducted experimental investigations after 8 h of aging at 500 °C, these precipitates had a diameter of about 5 nm to 15 nm.
5. Hafnium atoms segregated at the precipitate–matrix interface of Cr-containing particles. Increased hafnium concentrations next to these chromium phases lowered the necessary effort for intermetallic CuHf phases to precipitate, acting like a potent heterogeneous nucleation site. As a result, many intermetallic CuHf precipitates saddled on top of the existing chromium particles. The finely distributed precipitates resulted in excellent mechanical properties with less overaging and good electrical conductivities.

The thorough discussion in this research contributes to the understanding of alloy design and processing on precipitating copper alloys containing hafnium and chromium. Especially target-oriented alloy design is the highlight of effectively utilizing beneficial precipitation processes and high hardening potential simultaneously, which had not been discussed in the literature so far. Copper alloys, which utilize mainly Cr-containing precipitates to facilitate a homogenously distributed precipitation of high-strength intermetallic CuHf phases, provide high potential for further research on advanced applications.

Supplementary Materials: The following supporting information can be downloaded at: https://www.mdpi.com/article/10.3390/met14030258/s1, Video S1: Atom probe tomography of CuHf0.7Cr0.35 after 8 h aging at 500 °C with 10,000 Cu visualized, chromium and hafnium atoms (Video).

Author Contributions: Conceptualization, J.D., M.K., U.P., H.W.H. and A.Z.; methodology, J.D., M.K., B.O., P.O. and S.F.K.; investigation, J.D., M.K., B.O., P.O. and S.F.K.; resources, H.W.H., M.F. and A.Z.; writing—original draft preparation, J.D., M.K. and P.O.; writing—review and editing, H.W.H., U.P. and A.Z.; visualization, J.D., M.K. and P.O.; supervision, H.W.H., U.P., M.F. and A.Z. All authors have read and agreed to the published version of the manuscript.

Funding: This research received no external funding.

Data Availability Statement: The original contributions presented in the study are included in the article/Supplementary Materials, further inquiries can be directed to the corresponding author.

Conflicts of Interest: The authors declare no conflict of interest.

Appendix A

The discussed SEM analysis was conducted to examine the precipitation behavior during DSC experiments. This visualized the physical boundaries of the utilized experimental setup. For both conditions (heating to 590 °C and 700 °C), the structures related to intermetallic CuHf precipitates are visible with a nice bright contrast in the backscatter detector (BSD) of Figure A1. Energy-dispersive X-ray spectroscopy (EDS) enabled to contrast the enhanced hafnium concentration only if the structures were coarsened, whereas the chromium distribution was homogenous for all conditions.

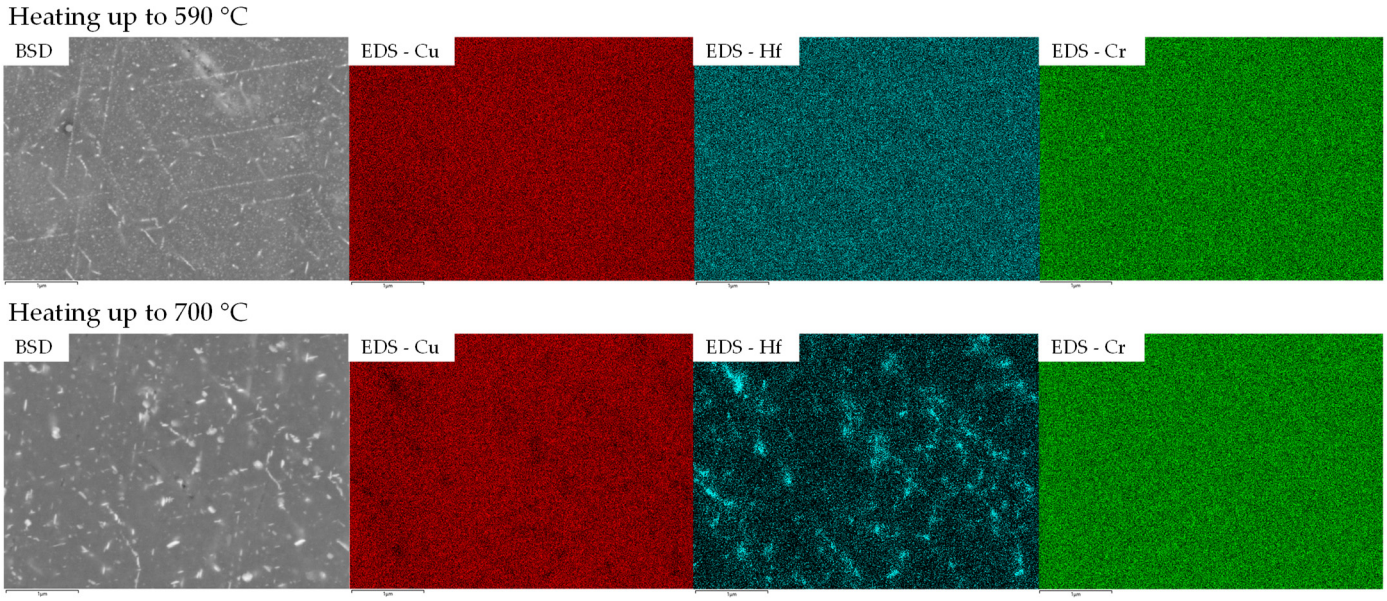

Figure A1. EDS analysis of CuHf0.7Cr0.35 following the precipitation process during the conducted DSC experiments.

References

1. Davis, J.R. *Metals Handbook: Non-Ferrous Alloys and Special-Purpose Materials*, 10th ed.; ASM International: Materials Park, OH, USA, 1990; ISBN 0871703785.
2. Dies, K. *Kupfer und Kupferlegierungen in der Technik*; Springer: Berlin/Heidelberg, Germany, 2014; ISBN 978-3-642-48932-7.
3. Gottstein, G. *Materialwissenschaft und Werkstofftechnik: Physikalische Grundlagen*, 4th ed.; Springer: Berlin/Heidelberg, Germany, 2014; ISBN 978-3-642-36602-4.
4. Porter, D.A.; Easterling, K.E.; Sherif, M.Y. (Eds.) *Phase Transformations in Metals and Alloys*, 4th ed.; CRC Press: Boca Raton, FL, USA, 2021; ISBN 9781003011804.
5. Kupferinstitut, D. Niedriglegierte Kupferwerkstoffe: Eigenschaften-Verarbeitung-Verwendung. *TechnologieForum Kupfer* **2012**, *8*, 1–36.
6. Dölling, J.; Kracun, S.F.; Prahl, U.; Fehlbier, M.; Zilly, A. A Comparative Differential Scanning Calorimetry Study of Precipitation Hardenable Copper-Based Alloys with Optimized Strength and High Conductivity. *Metals* **2023**, *13*, 150. [CrossRef]
7. Li, M.; Zhang, L.; Zhu, M.; Wang, H.; Wei, H. Physical Properties and Precipitate Microstructures of Cu-Hf Alloys at Different Processing Stages. *Scanning* **2018**, *2018*, 3653987. [CrossRef] [PubMed]
8. Freudenberger, J.; Heilmaier, M. *Materialkunde der Nichteisenmetalle und -Legierungen*, 1st ed.; Wiley-VCH Verlag GmbH & Co. KGaA: Weinheim, Germany, 2020; ISBN 9783527822546.
9. Chakrabarti, D.J.; Laughlin, D.E. The Cr-Cu (Chromium-Copper) system. *Bull. Alloy Phase Diagr.* **1984**, *5*, 59–68. [CrossRef]
10. Li, H.; Xie, S.; Wu, P.; Mi, X. Study on improvement of conductivity of Cu-Cr-Zr alloys. *Rare Met.* **2007**, *26*, 124–130. [CrossRef]
11. Peng, L.; Xie, H.; Huang, G.; Xu, G.; Yin, X.; Feng, X.; Mi, X.; Yang, Z. The phase transformation and strengthening of a Cu-0.71 wt% Cr alloy. *J. Alloys Compd.* **2017**, *708*, 1096–1102. [CrossRef]
12. Chbihi, A.; Sauvage, X.; Blavette, D. Atomic scale investigation of Cr precipitation in copper. *Acta Mater.* **2012**, *60*, 4575–4585. [CrossRef]
13. Liu, J.; Hou, M.; Yang, H.; Xie, H.; Yang, C.; Zhang, J.; Feng, Q.; Wang, L.; Meng, L.; Wang, H. In-situ TEM study of the dynamic interactions between dislocations and precipitates in a Cu-Cr-Zr alloy. *J. Alloys Compd.* **2018**, *765*, 560–568. [CrossRef]
14. Wan, X.; Xie, W.; Chen, H.; Tian, F.; Wang, H.; Yang, B. First-principles study of phase transformations in Cu–Cr alloys. *J. Alloys Compd.* **2021**, *862*, 158531. [CrossRef]
15. Bodyakova, A.; Mishnev, R.; Belyakov, A.; Kaibyshev, R. Effect of chromium content on precipitation in Cu–Cr–Zr alloys. *J. Mater. Sci.* **2022**, *57*, 13043–13059. [CrossRef]
16. Holzwarth, U.; Stamm, H. The precipitation behaviour of ITER-grade Cu–Cr–Zr alloy after simulating the thermal cycle of hot isostatic pressing. *J. Nucl. Mater.* **2000**, *279*, 31–45. [CrossRef]
17. Liu, Q.; Zhang, X.; Ge, Y.; Wang, J.; Cui, J.-Z. Effect of processing and heat treatment on behavior of Cu-Cr-Zr alloys to railway contact wire. *Metall. Mater. Trans. A* **2006**, *37*, 3233–3238. [CrossRef]
18. Abib, K.; Larbi, F.H.; Rabahi, L.; Alili, B.; Bradai, D. DSC analysis of commercial Cu–Cr–Zr alloy processed by equal channel angular pressing. *Trans. Nonferrous Met. Soc. China* **2015**, *25*, 838–843. [CrossRef]
19. Bourezg, Y.I.; Abib, K.; Azzeddine, H.; Bradai, D. Kinetics of Cr clustering in a Cu-Cr-Zr alloy processed by equal-channel angular pressing: A DSC study. *Thermochim. Acta* **2020**, *686*, 178550. [CrossRef]
20. Caron, R.N.; Sharif, A. Copper Alloys: Properties and Applications. In *Reference Module in Materials Science and Materials Engineering*; Hashmi, S., Ed.; Elsevier: Amsterdam, The Netherlands, 2017.
21. Zeiger, H. Stand und Entwicklung auf dem Gebiet der Kupferwerkstoffe. *Mater. Werkst.* **1986**, *17*, 75–78. [CrossRef]
22. Zhang, S.; Li, R.; Kang, H.; Chen, Z.; Wang, W.; Zou, C.; Li, T.; Wang, T. A high strength and high electrical conductivity Cu-Cr-Zr alloy fabricated by cryorolling and intermediate aging treatment. *Mater. Sci. Eng. A* **2017**, *680*, 108–114. [CrossRef]
23. Wang, H.; Gong, L.; Liao, J.; Chen, H.; Xie, W.; Yang, B. Retaining meta-stable fcc-Cr phase by restraining nucleation of equilibrium bcc-Cr phase in CuCrZrTi alloys during ageing. *J. Alloys Compd.* **2018**, *749*, 140–145. [CrossRef]
24. Hatakeyama, M.; Toyama, T.; Yang, J.; Nagai, Y.; Hasegawa, M.; Ohkubo, T.; Eldrup, M.; Singh, B.N. 3D-AP and positron annihilation study of precipitation behavior in Cu–Cr–Zr alloy. *J. Nucl. Mater.* **2009**, *386–388*, 852–855. [CrossRef]
25. Jiang, Y.; Zhang, X.; Cai, P.; Li, P.; Cao, F.; Gao, F.; Liang, S. Precipitation behavior and microstructural evolution during thermo-mechanical processing of precipitation hardened Cu-Hf based alloys. *Acta Mater.* **2023**, *245*, 118659. [CrossRef]
26. Okamoto, H. Cu-Hf (Copper-Hafnium). *J. Phase Equilib. Diffus.* **2007**, *28*, 583–584. [CrossRef]
27. Watanabe, R. Study on Copper-Rich Copper-Hafnium Alloys. *J. Jpn. Inst. Met.* **1966**, *30*, 754–759. [CrossRef]
28. Saarivirta, M.J. High conductivity copper alloys—Part 2. *Met. Ind.* **1963**, *103*, 716–718.
29. Saarivirta, M.J. High conductivity copper alloys—Part 3. *Met. Ind.* **1963**, *103*, 758–760.
30. Ghosh, G. First-principles calculations of structural energetics of Cu–TM (TM = Ti, Zr, Hf) intermetallics. *Acta Mater.* **2007**, *55*, 3347–3374. [CrossRef]
31. Bever, M.B.; Holt, D.L.; Titchener, A.L. The stored energy of cold work. *Prog. Mater. Sci.* **1973**, *17*, 5–177. [CrossRef]
32. Kodetová, V.; Vlach, M.; Čížek, J.; Cieslar, M.; Bajtošová, L.; Kudrnová, H.; Leibner, M.; Šíma, V. Early Stages of Precipitation in Mould-Cast, Cold-Rolled and Heat-Treated Aluminium Alloy AA7075 with Sc,Zr-Addition. *Acta Phys. Pol. A* **2020**, *137*, 250–254. [CrossRef]
33. Quainoo, G.K.; Yannacopoulos, S. The effect of cold work on the precipitation kinetics of AA6111 aluminum. *J. Mater. Sci.* **2004**, *39*, 6495–6502. [CrossRef]

34. Long, D.C.; Ohmori, Y.; Nakai, K. Effects of Cold Rolling on the Aging Kinetics in an Al–Mg–Si Based Commercial Alloy. *Mater. Trans. JIM* **2000**, *41*, 690–695. [CrossRef]
35. Naimi, A.; Yousfi, H.; Trari, M. Influence of cold rolling degree and ageing treatments on the precipitation hardening of 2024 and 7075 alloys. *Mech. Time-Depend. Mater.* **2013**, *17*, 285–296. [CrossRef]
36. Panigrahi, S.K.; Jayaganthan, R.; Pancholi, V.; Gupta, M. A DSC study on the precipitation kinetics of cryorolled Al 6063 alloy. *Mater. Chem. Phys.* **2010**, *122*, 188–193. [CrossRef]
37. Saarivirta, M.J. High conductivity copper alloys—Part 1. *Met. Ind.* **1963**, *103*, 685–688.
38. Yang, Y.; Kuang, G.; Li, R. Optimizing the Electrical and Mechanical Properties of Cu-Cr Alloys by Hf Microalloying. *Metals* **2022**, *12*, 485. [CrossRef]
39. Dobatkin, S.V.; Shangina, D.V.; Bochvar, N.R.; Terent'ev, V.F.; Prosvirnin, D.V.; Putinceva, M.N.; Purcek, G.; Yanar, H.; Alsaran, A.; Raab, G.I. Enhanced mechanical and service properties of ultrafinegrained copper-based alloys with Cu, Zr and Hf additives. *Mater. Sci. Non-Equilib. Phase Transform.* **2017**, *3*, 3–5.
40. Shangina, D.V.; Bochvar, N.R.; Dobatkin, S.V. The effect of alloying with hafnium on the thermal stability of chromium bronze after severe plastic deformation. *J. Mater. Sci.* **2012**, *47*, 7764–7769. [CrossRef]
41. Shangina, D.; Maksimenkova, Y.; Bochvar, N.; Serebryany, V.; Raab, G.; Vinogradov, A.; Skrotzki, W.; Dobatkin, S. Influence of alloying with hafnium on the microstructure, texture, and properties of Cu–Cr alloy after equal channel angular pressing. *J. Mater. Sci.* **2016**, *51*, 5493–5501. [CrossRef]
42. Shangina, D.; Maksimenkova, Y.; Bochvar, N.; Serebryany, V.; Raab, G.; Vinogradov, A.; Skrotzki, W.; Dobatkin, S. Structure and Properties of Cu Alloys Alloying with Cr and Hf after Equal Channel Angular Pressing. *Adv. Mater. Res.* **2014**, *922*, 651–656. [CrossRef]
43. Shangina, D.V.; Terent'ev, V.F.; Prosvirnin, D.V.; Antonova, O.V.; Bochvar, N.R.; Gorshenkov, M.V.; Raab, G.I.; Dobatkin, S.V. Mechanical Properties, Fatigue Life, and Electrical Conductivity of Cu-Cr-Hf Alloy after Equal Channel Angular Pressing. *Adv. Eng. Mater.* **2018**, *20*, 1700536. [CrossRef]
44. Bochvar, N.R.; Rybalchenko, O.V.; Shangina, D.V.; Dobatkin, S.V. Effect of equal-channel angular pressing on the precipitation kinetics in Cu-Cr-Hf alloys. *Mater. Sci. Eng. A* **2019**, *757*, 84–87. [CrossRef]
45. Falahutdinov, R.M.; Popov, V.V.; Popova, E.N.; Stolbovsky, A.V.; Shorokhov, E.V.; Gaan, K.V. The Effect of the Initial State on the Structure Evolution of Hafnium Bronze under Annealing. *Phys. Metals Metallogr.* **2022**, *123*, 900–907. [CrossRef]
46. Rybalchenko, O.V.; Bochvar, N.R.; Rybalchenko, G.V.; Martynenko, N.S.; Tabachkova, N.Y.; Dobatkin, S.V. Comparative analysis of the aging kinetics in low-alloyed Cu–Cr–Hf and Cu–Cr–Zr alloys after high pressure torsion. *J. Alloys Compd.* **2023**, *955*, 170246. [CrossRef]
47. Dölling, J.; Henle, R.; Prahl, U.; Zilly, A.; Nandi, G. Copper-Based Alloys with Optimized Hardness and High Conductivity: Research on Precipitation Hardening of Low-Alloyed Binary CuSc Alloys. *Metals* **2022**, *12*, 902. [CrossRef]
48. Dölling, J.; Zilly, A. Niedriglegierte festigkeitsoptimierte Kupferbasislegierungen mit hohen Leitfähigkeitseigenschaften: Untersuchung des Potentials binärer CuSc-Legierungen. In Proceedings of the Kupfer-Symposium 2021 Tagungsbeiträge, Werkstofftagung. Kupfer-Symposium, Jena, Germany, 24–25 November 2021; Deutsches Kupferinstitut, E.V., Ed.; 2021; pp. 16–19.
49. Henle, R.; Dölling, J.; Prahl, U.; Nandi, G.; Zilly, A. DSC Analysis of the Effect of Cold Deformation on the Precipitation Kinetics of a Binary Cu-Sc Alloy. *Materials* **2023**, *16*, 3462. [CrossRef] [PubMed]
50. Birol, Y. DSC analysis of the precipitation reaction in AA6005 alloy. *J. Therm. Anal. Calorim.* **2008**, *93*, 977–981. [CrossRef]
51. Li, X.; Starink, M.J. Analysis of Precipitation and Dissolution in Overaged 7xxx Aluminium Alloys Using DSC. *Mater. Sci. Forum* **2000**, *2000*, 1071–1076. [CrossRef]
52. Vončina, M.; Medved, J.; Kores, S.; Xie, P.; Schumacher, P.; Li, J. Precipitation microstructure in Al-Si-Mg-Mn alloy with Zr additions. *Mater. Charact.* **2019**, *155*, 109820. [CrossRef]
53. Ceguerra, A.V.; Breen, A.J.; Stephenson, L.T.; Felfer, P.J.; Araullo-Peters, V.J.; Liddicoat, P.V.; Cui, X.; Yao, L.; Haley, D.; Moody, M.P.; et al. The rise of computational techniques in atom probe microscopy. *Curr. Opin. Solid State Mater. Sci.* **2013**, *17*, 224–235. [CrossRef]
54. Yoo, S.-H.; Kim, S.-H.; Woods, E.; Gault, B.; Todorova, M.; Neugebauer, J. Origins of the hydrogen signal in atom probe tomography: Case studies of alkali and noble metals. *New J. Phys.* **2022**, *24*, 13008. [CrossRef]
55. Felfer, P. *Atom-Probe-Toolbox*; Github; FAU Erlangen: Erlangen-Nürnberg, Germany, 2023.
56. Felfer, P.; Ceguerra, A.V.; Ringer, S.P.; Cairney, J.M. Detecting and extracting clusters in atom probe data: A simple, automated method using Voronoi cells. *Ultramicroscopy* **2015**, *150*, 30–36. [CrossRef] [PubMed]
57. Miyake, J.; Fine, M.E. Electrical conductivity versus strength in a precipitation hardened alloy. *Acta Metall. Mater.* **1992**, *40*, 733–741. [CrossRef]
58. Naboka, M.; Giordano, J. (Eds.) *High Strengh Copper-Based Conductor Materials*; Nova Science Publishers: Hauppauge, NY, USA, 2011; ISBN 9781612095042.
59. Dalan, F.C.; de Lima Andreani, G.F.; Travessa, D.N.; Faizova, S.; Fiazov, I.A.; Cardoso, K.R. Effect of ECAP Processing on Hardness, Electrical Conductivity, and Precipitation Kinetics of the Cu-0.81Cr-0.07Zr Alloy. *J. Electron. Mater.* **2021**, *50*, 6171–6182. [CrossRef]
60. Füssel, U.; Jüttner, S. *Lebensdauererhöhung von Widerstandspunktschweißelektroden durch Einsatz verschleißabhängiger Fräsintervalle und dispersionsgehärteter Kupferwerkstoffe: Schlussbericht zu IGF-Vorhaben Nr. 18.456: Berichtszeitraum: 01.07.2015–30.09.2017*; Industrielle Gemeinschaftsforschung: Magdeburg, Germany, 2018.

61. Fukumoto, S.; Lum, I.; Biro, E.; Boomer, D.R.; Zhou, Y. Effects of Electrode Degradation on Electrode Life in Resistance Spot Welding of Aluminum Alloy 5182. *Weld. J.* **2003**, *82*, 307s–312s.
62. Shangina, D.V.; Ivanov, N.I.; Bochvar, N.R.; Dobatkin, S.V. Resistance of the Contact Welding Electrodes Made of a Cu–0.7% Cr–0.9% Hf Alloy with an Ultrafine-Grained Structure. *Russ. Metal.* **2018**, *2018*, 815–819. [CrossRef]
63. AMI Doduco. *Datenbuch der Elektrischen Kontakte*, 3rd ed.; AMI Doduco GmbH: Pforzheim, Germany, 2009.
64. Mroczkowski, R.S.; Jugy, R.; Gerfer, A. (Eds.) *Triologie der Steckverbinder: Applikationshandbuch zur Optimierten Steckverbinderauswahl*, 3rd ed.; Swiridoff: Künzelsau, Germany, 2016; ISBN 978-3-89929-200-8.
65. Katzier, H. *Elektrische Steckverbinder: Technologien, Anwendungen und Anforderungen; mit 60 Tabellen, 1. Auflage*; Leuze: Bad Saulgau, Germany, 2012; ISBN 9783874802734.
66. KME Germany GmbH & Co., K.G. *KME Kupferpulver: Materialdatenblatt*; KME Germany GmbH & Co. KG: Osnabrück, Germany, 2022.
67. Poltz, I.; Jürgens, P.; Blüm, M.; Weber, S. Additive Fertigung von CuSn11 Werkstoffen mit selektivem Laserschmelzen (SLM). *Metall* **2016**, *70*, 438–442.
68. Fraunhofer Gesellschaft e.V. *Fraunhofer-Institut für Lasertechnik ILT. Schlussbericht zu IGF-Vorhaben Nr. 19.549 N: Additive Fertigung von Bauteilen aus Rein-Kupfer mittels SLM und "grüner" Laserstrahlung*; Industrielle Gemeinschaftsforschung: Aachen, Germany, 2020.
69. Tiberto, D.; Klotz, U.E.; Held, F.; Wolf, G. Additive manufacturing of copper alloys: Influence of process parameters and alloying elements. *Mater. Sci. Technol.* **2019**, *35*, 969–977. [CrossRef]
70. Popovich, A.; Sufiiarov, V.; Polozov, I.; Borisov, E.; Masaylo, D.; Orlov, A. Microstructure and mechanical properties of additive manufactured copper alloy. *Mater. Lett.* **2016**, *179*, 38–41. [CrossRef]
71. Silbernagel, C.; Gargalis, L.; Ashcroft, I.; Hague, R.; Galea, M.; Dickens, P. Electrical resistivity of pure copper processed by medium-powered laser powder bed fusion additive manufacturing for use in electromagnetic applications. *Addit. Manuf.* **2019**, *29*, 100831. [CrossRef]
72. Ellis, D.L. *GRCop-84: A High-Temperature Copper Alloy for High-Heat-Flux Applications: 213566*; Glenn Research Center: Cleveland, OH, USA, 2005.
73. Tang, X.; Chen, X.; Sun, F.; Liu, P.; Zhou, H.; Fu, S. The current state of CuCrZr and CuCrNb alloys manufactured by additive manufacturing: A review. *Mater. Des.* **2022**, *224*, 111419. [CrossRef]
74. Uchida, S.; Kimura, T.; Nakamoto, T.; Ozaki, T.; Miki, T.; Takemura, M.; Oka, Y.; Tsubota, R. Microstructures and electrical and mechanical properties of Cu-Cr alloys fabricated by selective laser melting. *Mater. Des.* **2019**, *175*, 107815. [CrossRef]

Disclaimer/Publisher's Note: The statements, opinions and data contained in all publications are solely those of the individual author(s) and contributor(s) and not of MDPI and/or the editor(s). MDPI and/or the editor(s) disclaim responsibility for any injury to people or property resulting from any ideas, methods, instructions or products referred to in the content.